Energy Reports 9 (2023) 454–459

Contents lists available at ScienceDirect

Energy Reports

journal homepage: www.elsevier.com/locate/egyr

A combined *dq*-MIMO and sequence-SISO impedance-based stability assessment scheme for IBR interfaced system☆

Lei Meng [a], Tao Xue [a], Ulas Karaagac [a,*], Lijun Cai [b]

[a] Department of Electrical and Electronic Engineering, Hong Kong Polytechnic University, Kowloon, Hong Kong, China
[b] Institute for Electrical Power Engineering, University of Rostock, Rostock, Germany

ARTICLE INFO

Keywords:
Dq-MIMO impedance
EMT-type impedance scanning
Impedance-based stability assessment
Impedance transformation
Sequence-SISO impedance

ABSTRACT

The electromagnetic transient (EMT)-type impedance scanning methods conducted in positive sequence domain and dq-frame (p-scan and dq-scan, respectively) have been widely used for identifying inverter-based resource (IBR) instabilities. They obtain the sequence domain single-input single-output (sequence-SISO) and dq-frame multi-input multi-output (dq-MIMO) impedance models of an IBR, respectively. The dq-MIMO impedance-based stability assessment (IBSA) is more accurate compared to the sequence-SISO IBSA as it considers the mirror frequency effect (MFE). However, unlike the sequence-SISO, the dq-MIMO IBSA cannot differentiate the resonance frequency from its mirror frequency, because the dynamics in dq-frame incorporate both the positive and negative sequence impedances of IBR. This paper proposes a new IBSA scheme to eliminate this shortcoming. First, a dq-MIMO IBSA is carried out to obtain the accurate dq-frame resonance frequency and stability margin. Then a sequence-SISO IBSA is conducted to determine the phase domain resonance frequency. The sequence-SISO impedance models are transformed from the dq-MIMO model. The proposed scheme has lower computational costs than the existing dq-MIMO IBSA methods. The effectiveness of the proposed scheme is validated on a test system incorporating full-size converter-based wind park (FSC-based WP). This paper also demonstrates the possibility of weak grid instability occurrence in supersynchronous frequency range.

1. Introduction

In the past decades, electrical supplies around the world have been increasingly comprised by renewable energy resources such as solar, wind, hydropower, and battery systems. These resources are normally integrated into the electrical power grids through power electronic inverters, thus, are called inverter-based resources (IBRs) (Gu and Green, 2022). However, incidents related to IBRs have been reported all over the world, and studies have demonstrated that the IBR controllers can adversely interact with the transmission grid (Cheng et al., 2023; IEEE-PES Wind SSO Task Force, 2020). In order to investigate the IBRs related stability issue, different methods have been used, including the eigenvalue analysis (Karaagac et al., 2018; Fan and Miao, 2018; Pogaku et al., 2007), impedance-based stability assessment (IBSA) (Cespedes and Sun, 2014; Badrzadeh et al., 2013; Cheng et al., 2013; Wen et al., 2015; Trevisan et al., 2021; Huang et al., 2009; Rygg et al., 2016; Ren and Larsen, 2016), and electromagnetic transient (EMT) simulations (Watson and Arrillaga, 2003), (Xie et al., 2012). The eigenvalue analysis could interpret the instability mechanism using the participation of each state variable to the dominant eigenvalues (Pogaku et al., 2007). However, it is oversimplified during the linearization, thus, has accuracy issue (Karaagac et al., 2018; Fan and Miao, 2018; Pogaku et al., 2007). Moreover, it is not accessible to manufacturer-specific models (i.e., black-box models) (Trevisan et al., 2021).

IBSA recently became popular in identifying IBR instabilities due to its simplicity and applicability to large-scale power systems (IEEE-PES Wind SSO Task Force, 2020; Cheng et al., 2019). The expected accuracy for obtaining the frequency dependent impedance model of IBR can be achieved by using a EMT-type impedance scanning method (Karaagac et al., 2018; Badrzadeh et al., 2013; Cheng et al., 2013; Wen et al., 2015; Trevisan et al., 2021; Huang et al., 2009). This method is also valid for manufacturer-specific models. The EMT simulations are usually performed in representative scenarios to validate the eigenvalue analysis or IBSA results.

The EMT-type positive-sequence impedance scanning (p-scan) method is widely used for measuring the positive sequence impedance

☆ 2023 8th International Conference on Sustainable and Renewable Energy Engineering (ICSREE 2023) 11–13 May, Nice, France.

* Corresponding author.
E-mail address: ulas.karaagac@polyu.edu.hk (U. Karaagac).

https://doi.org/10.1016/j.egyr.2023.12.006
Received 1 November 2023; Accepted 1 December 2023
Available online 8 December 2023

models of IBRs (IEEE-PES Wind SSO Task Force, 2020; Karaagac et al., 2018; Badrzadeh et al., 2013; Cheng et al., 2013). However, the usage of the obtained sequence-domain single-input single-output (sequence--SISO) impedance model in IBSA has accuracy issue as the mirror frequency effect (MFE) in IBR is ignored (Rygg et al., 2016; Ren and Larsen, 2016). The MFE is caused by the asymmetry in IBR impedance model, due to the phase locked loop (PLL) and different outer-loop control strategies in d- and q-axis (Ren and Larsen, 2016). The dq-frame impedance scanning (dq-scan) is developed to take the asymmetry and couplings in dq-frame multi-input multi-output (dq-MIMO) impedances/admittances of IBRs (Wen et al., 2015; Trevisan et al., 2021; Huang et al., 2009), thus, the MFE is inherently accounted.

On the other hand, as the dq-MIMO IBSA is conducted in dq-frame, the obtained resonance frequency (f_{r-dq}) contains the information of both phase-domain resonance and mirror frequencies (f_r and f_m, respectively). Subtracting (adding) the fundamental frequency (f_b) from (to) f_{r-dq} will give either f_r or f_m. Identifying f_r and f_m requires EMT simulation of the entire system and the spectral analysis.

To eliminate the dependence of dq MIMO IBSA on the time consuming EMT simulation of the entire system, this letter proposes conducting sequence SISO IBSA after dq MIMO IBSA for identifying f_r. The impedance transformation between dq- and stationary decoupled sequence (sds)- frames are used to obtain the sequence-SISO impedance model for IBSA. Thus, the p-scan procedure is not required. Moreover, with the usage of phasor solution-based impedance scanning method in grid-side subsystem (Agrawal and Farmer, 1979) and the corresponding impedance transformation, the computational efficiency of the dq-MIMO IBSA is significantly improved compared with the existing dq-MIMO IBSA methods (Wen et al., 2015; Trevisan et al., 2021; Huang et al., 2009; Rygg et al., 2016). The proposed combined dq-MIMO and sequence-SISO IBSA method is conducted on a test system in which a large-scale full-size converter-based wind park (FSC-based WP) is weakly-tied to a transmission grid. Its effectiveness is validated through EMT simulations. Moreover, the weak grid instability is identified in supersynchronous rather than subsynchronous frequency range although a typical weak grid instability case is adopted. The mechanism of the FSC-based WP related weak grid issue and the possible reason of its misperception is also discussed.

The remaining part of this paper is organized as follows. Section 2 introduces the procedure of the proposed combined IBSA method and the theoretical basis of impedance transformation. Section 3 presents the EMT validation and discusses the weak grid issue in super-synchronous frequency range. Section 4 concludes the paper.

2. The combined dq-MIMO and sequence-SISO impedance-based stability assessment

The flow chart of the proposed IBSA scheme is presented in Fig. 1(a). In IBSA, the system under study should be separated into a grid- and IBR-side subsystems from their point of interconnection (PoI). The grid-side sequence-SISO impedance model is obtained with the phasor solution-based impedance scanning tool (Agrawal and Farmer, 1979) as it is unpractical to use the EMT-level impedance scanning method in large-scale systems (Cheng et al., 2019). The IBR-side dq MIMO impedance is obtained through the EMT-level dq-scan. The procedures of the proposed method are as follows.

2.1. IBR-side impedance measurement and processing

2.1.1. IBR-side dq-scan

The schematic diagram of dq-scan for IBR is presented in Fig. 1(b). The grid-side subsystem should be represented by an ideal voltage source ($\mathbf{v}_{\mathbf{Sys}}$) behind the fundamental frequency Thevenin equivalent impedance of the system ($\mathbf{Z}_{\mathbf{Sys}}(f_b) = \mathbf{R}_{\mathbf{Sys}}(f_b) + j\mathbf{X}_{\mathbf{Sys}}(f_b)$). A certain initialization time (T_0) is required for system reaches to a steady state condition, and a snapshot of the system is taken at the end of initialization. This snapshot is used in the following impedance scanning process, thus, re-initialization before each perturbation injection is not required. The voltage perturbations are used in this paper. The generic procedures are as follows:

Step a. The dq-frame single tone sinusoidal perturbation signals are generated and transformed into abc-domain. The perturbation voltage is

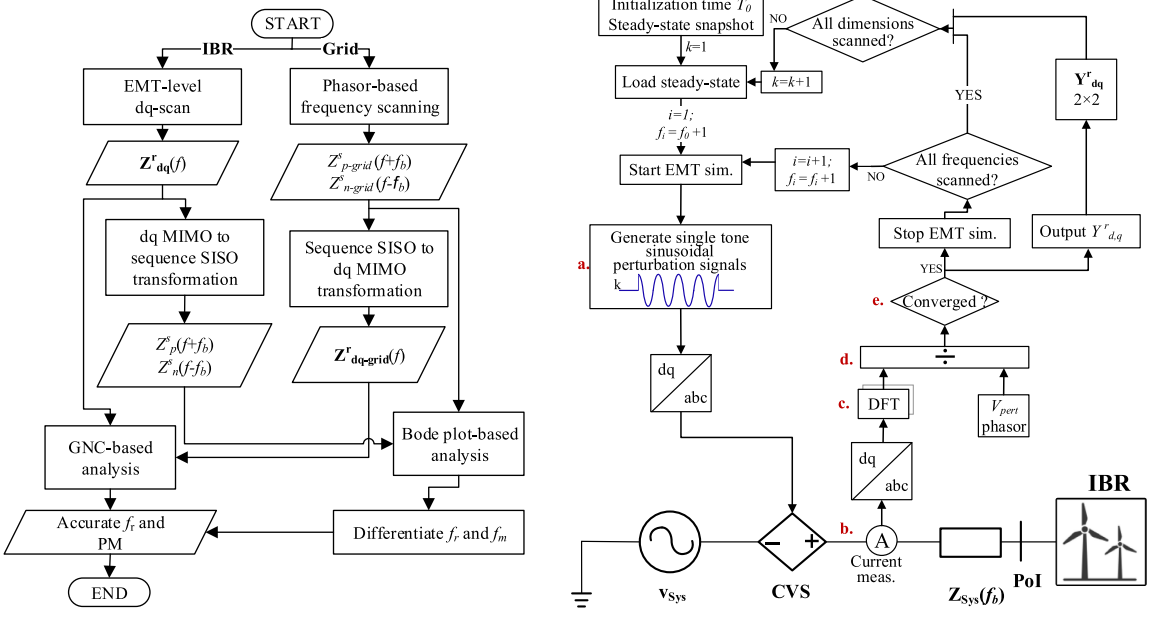

Fig. 1. (a) Flow chart of the combined dq-MIMO and sequence-SISO IBSA method. (b) dq-scan procedure for IBR.

added on top of the $\mathbf{v_{Sys}}$ through a series connected controlled voltage source (CVS).

Step b. The three-phase current signals are measured from the point of injection and transformed back to dq-frame.

Step c. The discrete Fourier transform (DFT) analysis extracts the frequency spectra of the measured current signals.

Step d. The dq-MIMO admittance of the IBR is calculated by:

$$\mathbf{Y^r_{dq}}(f_i) = \begin{bmatrix} Y^r_{d,d}(f_i) & Y^r_{d,q}(f_i) \\ Y^r_{q,d}(f_i) & Y^r_{q,q}(f_i) \end{bmatrix}, with Y^r_{j,k} = \frac{I^k_j}{V^k} \tag{1}$$

where $j,k \in \{d,\ q\}$. the superscript k in I^k_j and V^k indicates the axis of perturbation injection, and the subscript j in I^k_j indicates the axis of the measured current signal; the superscript 'r' in $\mathbf{Y^r_{dq}}$ and $Y^r_{j,k}$ denotes the synchronous rotating reference frame (SRRF).

Step e. A convergence test ensures the variation of each $\mathbf{Y^r_{dq}}$ component is negligible. The convergence criteria are:

$$\left| \frac{d\left|Y^r_{j,k}(f_i)\right|}{\left|Y^r_{j,k}(f_i)\right|} \right| < tol \quad \& \quad \left| \frac{d\ Ang\left(Y^r_{j,k}(f_i)\right)}{Ang\left(Y^r_{j,k}(f_i)\right)} \right| < tol \tag{2}$$

where $|\bullet|$ and $Ang\ (\bullet)$ are the magnitude and angle calculators, respectively; $d(\bullet)$ denotes variation with respect to user defined time step; *tol* is the convergence tolerance. Once the convergence criteria in (2) are fulfilled, the admittance data is saved for IBSA and the dq-scan procedure for f_i is stopped and is repeated for the next perturbation frequency.

Two sets of dq-frame perturbation signals between 1 and 59 Hz for a 60 Hz system are required to measure the dq-MIMO impedance of the IBR ($\mathbf{Z^r_{dq}}(f_i) = (\mathbf{Y^r_{dq}}(f_i))^{-1}$). Readers can find more details about dq-scan techniques in (Trevisan et al., 2021).

2.1.2. IBR-side impedance processing

The obtained IBR dq-MIMO impedance model is first converted into the SRRF coupled sequence impedance ($\mathbf{Z^r_{pn}}$)using a linear transformation (Rygg et al., 2016):

$$\mathbf{Z^r_{pn}}(f_i) = \begin{bmatrix} Z^r_{p,p}(f_i) & Z^r_{p,n}(f_i) \\ Z^r_{n,p}(f_i) & Z^r_{n,n}(f_i) \end{bmatrix} = \underbrace{\begin{bmatrix} 1 & j \\ 1 & -j \end{bmatrix}}_{\mathbf{C}} \mathbf{Z^r_{dq}}(f_i) \underbrace{\frac{1}{2}\begin{bmatrix} 1 & 1 \\ -j & j \end{bmatrix}}_{\mathbf{C^{-1}}} \tag{3}$$

Then, $\mathbf{Z^r_{pn}}(f_i)$ is transformed to SRF positive and negative sequence SISO models ($Z^s_p(f_i)$ and $Z^s_n(f_i)$, respectively) using (Rygg et al., 2016):

$$Z^s_p(f_i) = \det\left(\mathbf{Z^r_{pn}}(f_i - f_b)\right) \Big/ Z^r_{n,n}(f - f_b) \tag{4}$$

$$Z^s_n(f_i) = \det\left(\mathbf{Z^r_{pn}}(f_i + f_b)\right) \Big/ Z^r_{p,p}(f_i + f_b) \tag{5}$$

where det $(\bullet)$ denotes the determinant of matrix.

Eqs. (3)–(5) contain frequency shift relations between dq-MIMO and sequence-SISO impedances as illustrated in Fig. 2. $\mathbf{Z^r_{dq}}(f_i)$ (from 1 to 59 Hz) incorporates both $Z^s_p(f_i)$ (from 61 to 119 Hz) and $Z^s_n(f_i)$ (from −59 to −1 Hz). It should be noted that, $Z^s_n(f_i)$ from − 59 to − 1 Hz is equivalent to the conjugate of $Z^s_p(f_i)$ from 59 to 1 Hz. Hence, $Z^s_p(f_i)$ from 1 to 59 Hz can be simply obtained by rotating $Z^s_n(f_i)$ from - 1 to − 59 Hz with respect to 0 Hz axis as illustrated in Fig. 2. As a result, 1–119 Hz sequence-SISO impedance models are obtained from 1 to 59 Hz dq-MIMO impedance models. This approach takes about half of the simulation time of the method proposed in (Rygg et al., 2016) as it uses − 59–59 Hz dq MIMO impedances to obtain the 1–119 Hz positive sequence impedances.

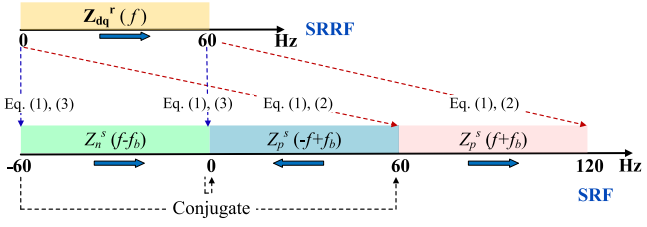

Fig. 2. The frequency shift relation in impedance transformation.

2.2. Grid-side impedance measurement and processing

The EMT-type impedance scanning is not practical for the grid-side impedance measurement due to its heavy computational burden. Hence, the phasor solution-based impedance scanning technique can be used to extract the grid-side sequence-SISO impedance models (Agrawal and Farmer, 1979). The grid-side subsystem may also have IBRs. These IBRs can be represented by their frequency dependent impedance tables, which were obtained from EMT-type impedance scanning (Cheng et al., 2019). The grid-side sequence-SISO impedance model needs to be transformed into its dq-MIMO equivalent using:

$$\mathbf{Z^r_{dq-grid}}(f_i) = \mathbf{C}^{-1} \begin{bmatrix} Z^s_{p-grid}(f_i + f_b) & \\ & Z^s_{n-grid}(f_i - f_b) \end{bmatrix} \mathbf{C} \tag{6}$$

where $\mathbf{Z^r_{dq-grid}}(f_i)$ is the grid-side dq-MIMO impedance model, which is a symmetric matrix; $Z^s_{p-grid}(f_i + f_b)$ and $Z^s_{n-grid}(f_i - f_b)$ are positive and negative sequence impedances of the grid-side subsystem in SRF, respectively.

2.3. Impedance-based stability assessment

The generalized Nyquist criterion (GNC) is typically used in dq-MIMO IBSA (Trevisan et al., 2021). The return ratio matrix of the integrated system is given as:

$$\mathbf{L}(s) = \mathbf{Z^r_{dq-grid}}(s)\mathbf{Y^r_{dq}}(s) \tag{7}$$

where $s = j2\pi f_i$. The closed-loop system is stable if the encirclement of all the eigenloci of $\mathbf{L}(s)$ to (−1, j0) is zero, under precondition of there are no open-loop poles in right half plane (RHP) (Webster et al., 2019).

The combined dq-MIMO and sequence-SISO IBSA is achieved as follows: 1) The GNC-based analysis finds f_{rdq} and the accurate stability margin of the system. 2) Then the Bode plot-based analysis (Liao and Wang, 2018) is conducted to find the intersection frequency (f_s) of Z^s_{p-grid} and Z^s_p in SRF, which helps to differentiate f_r and f_m.

3. Case study and validation

3.1. Test system

The benchmark of the adopted test system is presented in Fig. 3. The large-scale FSC-based WP contains 500 wind turbines (WTs, 1.5 MW each), and it connects with a 500 kV large system with two parallel lines. Each line is represented with an equivalent impedance (Z_1 and Z_2). The output active and reactive power of the FSC-based WP are 0.9 and 0 pu,

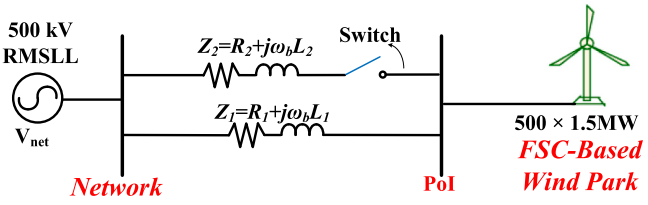

Fig. 3. System under study.

respectively. At beginning, the system is stable, and line 2 (Z_2) is disconnected at 5 s by opening the Switch. Due to this contingency, the total short circuit ratio (SCR) of the system reduces from 3.87 to 1.02 and leads to a weak grid issue. The FSCs are represented by their average value models (AVMs), important systematic and control parameters are presented in Table 1. Detailed model and control schemes of the FSC-based WP can be found in (Karaagac et al., 2019) and (Seyedi et al., 2022).

3.2. Instability identification

The EMT-type dq-scan of FSC-based WP is conducted in the EMTP within (Gu and Green, 2022; 59,) Hz frequency range (with 1 Hz resolution). The voltage perturbation amplitude is 0.01 pu, and the admittance convergence tolerance is 0.5%. The processor used for the computation is an Intel(R) Core (TM) i5–7600 3.50 GHz. The time step for all EMT simulations is 50 μs.

The obtained dq-MIMO impedance model of the WP is converted into sequence-SISO impedance models using Eqs. (3)–(5). The accuracy of the conversion is verified with the p-scan results as shown in the Bode plot in Fig. 4(b). The sequence-SISO impedances of the grid (Z_1) are transformed into dq-frame using Eq. (6). The GNC-based dq-MIMO IBSA identifies an instability at 48 Hz (f_{r-dq}) with a very low negative phase margin (PM) (-0.2°) as seen in Fig. 4(a). The sequence SISO IBSA indicates a stable intersection at 109.5 Hz with a very low positive PM (2.8°) as seen in Fig. 4(b). This small discrepancy is due to ignoring the MFE in sequence SISO IBSA, and it indicates the sequence SISO IBSA exhibits inaccuracy. Combining the dq-MIMO and sequence-SISO IBSA results, one can learn that the system has an unstable resonance at 108 Hz (f_r = 60 Hz + 48 Hz) with 12 Hz (f_m = 60–48 Hz) mirror frequency and -0.2° PM. As the grid and IBR sequence SISO impedance intersection frequencies at around 20 Hz and 60 Hz have large PMs ($>20^\circ$), instability can be expected only at 108 Hz.

The time domain simulation results are presented in Fig. 5. Growing oscillations are found in both the output active and reactive power of WT. FFT analysis finds oscillation components in GSC output voltage waveform at both 108 Hz and 12 Hz, and the 108 Hz component is significantly larger than the 12 Hz component. Thus, it determines that the instability occurs at 108 Hz. The time domain simulation validates the accuracy of the combined IBSA scheme and its effectiveness in differentiating f_r and f_m.

3.3. Discussion of the weak grid issue in super-synchronous frequency range

3.3.1. Mechanism of the FSC-based WP incorporated weak grid instability

The resistance-reactance plot (R-X plot) and the reactance crossover criterion (RCC) can be used to analyze the instability mechanism. The studied system is a balanced three-phase system and has no instability risks in the negative-sequence domain. Thus, the weak grid instability mechanism is analyzed with the positive sequence impedance model. The total positive sequence impedance of the FSC-based WP and the grid is given as:

$$Z_{total}(f_i) = R_{total}(f_i) + jX_{total}(f_i) = \big(R_{WP}(f_i) + R_{grid}(f_i)\big) + j\big(X_{WP}(f_i) + X_{grid}(f_i)\big) \tag{8}$$

where $R_{WP}(f_i)$, $R_{grid}(f_i)$ and $X_{WP}(f_i)$, $X_{grid}(f_i)$ are resistances and reactance of the WP and grid at frequency f_i, respectively. The RCC determines a system instability if the system total resistance and reactance at the reactance zero-crossover point (f_c) fulfills (Karaagac et al., 2018; Cheng et al., 2013):

$$R_{total}(f_c)\frac{dX_{total}(f_c)}{df_c} < 0 \tag{9}$$

The R-X plot of the FSC-based WP is shown in Fig. 6(a). It is capacitive in 1–13 Hz, 58–63 Hz, and 87–119 Hz frequency ranges, thus, may interact with the inductive grid impedance (Z_1) in these frequency ranges. According to Eq. (9), the system is safe from the unstable oscillation in the subsynchronous range, as in 1–13 Hz and 58–59 Hz the FSC-based WP has positive and negative reactance derivatives and positive and negative resistances, respectively. However, in the super-synchronous range, i.e., 100–110 Hz (encircled in dashed green rectangle), the WP has capacitive reactance (with positive derivative) and negative resistance, thus is vulnerable to unstable interaction with the inductive grid. The total impedance model of the FSC-based WP and Z_1 shown in Fig. 6(b) validates the analysis above. It is worth noting that the system is also be vulnerable to unstable oscillation in the super-synchronous frequency range close to the fundamental frequency, i.e., 61–63 Hz, under extreme weak grid conditions (very low SCR), whereas in sub-synchronous frequency range it has no weak grid instability risks.

In conclusion, classifying the FSC-associated weak grid instability as subsynchronous interaction (SSI) might be a misperception, possible reasons could be: 1) The analytical analyses were conducted in dq-frame, and the resonance frequency was directly reckoned as $f_r = f_b - f_{r-dq}$; 2) In the real-world incidents, the oscillations were detected by the root mean square (RMS) measurement, which only presents the distances between the oscillation and fundamental frequencies, i.e., $|f_b - f_r| = |f_b - f_m|$; 3) The amplitude of mirror frequency component is relatively high in specific incidents.

Table 1
Parameters of the Test System.

Item	Param./ Expr.	Value	Item	Param. / Expr.	Value
Power base	S_{base}	833.5 MVA	Z_2	$\lvert R_2+j\omega_b L_2\rvert$	0.39 p.u.
Voltage base	V_{base}	500 kV RMSLL		$R_2/\omega_b L_2$	0.1
Wind speed	v_{wind}	11.24 m/s	WT Nominal voltage	V_{WT}	575 V RMSLL
Z_1	$\lvert R_1+j\omega_b L_1\rvert$	1.02 p.u.	GSC inner loop rise time	$t_{r\text{-}GSC}$	i_d: 4 ms; i_q: 7 ms
	$R_1/\omega_b L_1$	0.1	GSC dc-voltage time constant	t_{dc}	150 ms

Note: $\omega_b = 2\pi f_b$ is the angular fundamental frequency; GSC: grid side converter.

4. Conclusion

In this paper, a combined dq-MIMO and sequence-SISO IBSA scheme is proposed, its effectiveness was demonstrated on a typical weak grid instability case. The contributions in this work are summarized as follows:

(1) The proposed scheme fixed the main drawback of the existing dq-scan and dq-MIMO IBSA as differentiating the resonance and mirror frequencies does not require time consuming EMT-simulation of the entire system and associated spectral analysis.
(2) With the usage of the phasor solution-based impedance scanning method in the grid-side subsystem, and impedance transformation for both grid-side sequence-SISO and IBR-side dq-MIMO impedance models, the proposed scheme significantly reduced the computational cost of IBSA.
(3) The FSC-associated weak grid instability was discussed from a new perspective. Although a typical weak grid instability case was adopted as a test system, the instability occurred in super-synchronous rather than subsynchronous frequency range. The weak grid instability was classified as SSI, but the instability might occur beyond the subsynchronous range. It was suggested

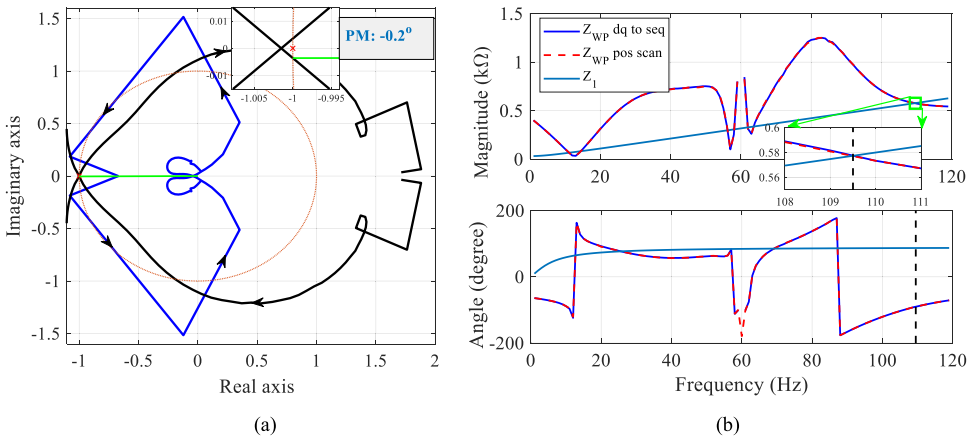

Fig. 4. (a) Nyquist diagram based on dq-MIMO impedance model (b) Bode plot of sequence-SISO impedance models.

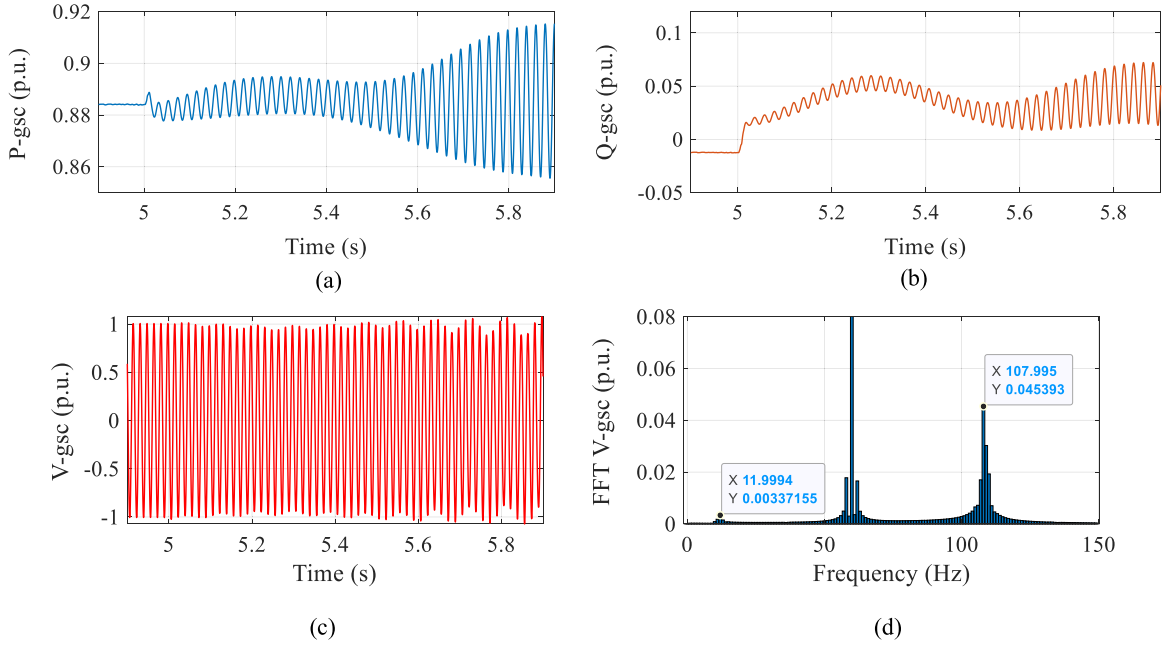

Fig. 5. EMT simulations: (a) GSC active power, (b) GSC reactive power, (c) GSC phase-a voltage, (d) frequency spectrum of the phase-a voltage waveform.

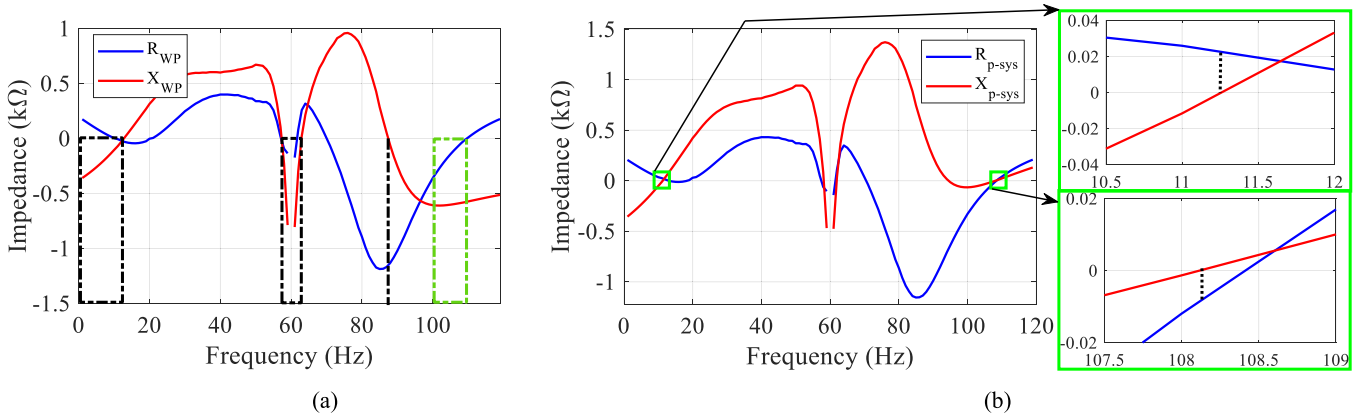

Fig. 6. (a) R-X plot of the FSC-based WP impedance. (b) R-X plot of the total impedance of the FSC-based WP and grid.

that the weak grid instability phenomenon should be deeply analyzed, and its classification needs to be updated.

Declaration of Competing Interest

The authors declare no conflict of interest.

Data Availability

Data will be made available on request.

Acknowledgements

This work was supported by the Hong Kong Research Grant Council for the Research Project under Grant 25223118.

References

Agrawal, B.L., Farmer, R.G., 1979. Use of frequency scanning techniques for subsynchronous resonance analysis. IEEE Trans. Power Appar. Syst. PAS-98.2 (1979), 341–349.

Badrzadeh, B., Sahni, M., Zhou, Y., Muthumuni, D., Gole, A., 2013. General methodology for analysis of sub-synchronous interaction in wind power plants. IEEE Trans. Power Syst. 28. 2 (2013), 1858–1869.

Cespedes, M., Sun, J., 2014. Impedance modeling and analysis of grid-connected voltage-source converters. IEEE Trans. Power Electron. 29 3 (2014), 1254–1261.

Cheng, Y., et al., 2023. Real-world subsynchronous oscillation events in power grids with high penetrations of inverter-based resources. IEEE Trans. Power Syst. 38.1 (2023), 316–330.

Cheng, Y., Sahni, M., Muthumuni, D., Badrzadeh, B., 2013. Reactance scan crossover-based approach for investigating SSCI concerns for DFIG-based wind turbines. IEEE Trans. Power Deliv. 28.2 (2013), 742–751.

Cheng, Y., Huang, S.H., (Fred), Rose, J., Pappu, V.A., Conto, J., 2019. Subsynchronous resonance assessment for a large system with multiple series compensated transmission circuits. IET Renew. Power Gener. 13 (1), 27–32, 2019.

Fan, L., Miao, Z., 2018. An explanation of oscillations due to wind power plants weak grid interconnection. IEEE Trans. Sustain. Energy 9.1, 488–490.

Y. Gu and T.C. Green. (2022) "Power System Stability With a High Penetration of Inverter-Based Resources," in Proceedings of the IEEE, (2022), doi: 10.1109/JPROC.2022.3179826.

Huang, J., Corzine, K.A., Belkhayat, M., 2009. Small-signal impedance measurement of power-electronics-based AC power systems using line-to-line current injection. IEEE Trans. Power Syst. 24.2, 445–455.

IEEE-PES Wind SSO Task Force, 2020. Wind energy systems sub-synchronous oscillations: events and modelling. Tech. Rep., PES-TR80, *AMPS Comm.* (2020).

Karaagac, U., et al., 2019. A generic EMT-type simulation model for wind parks with permanent magnet synchronous generator full size converter wind turbines. IEEE Power Energy Technol. Syst. J. 6. 3 (2019), 131–141.

Karaagac, U., Mahseredjian, J., Jensen, S., Gagnon, R., Fecteau, M., Kocar, I., 2018. Safe operation of DFIG-based wind parks in series-compensated systems. IEEE Trans. Power Deliv. 33.2 (2018), 709–718.

Y. Liao and X. Wang, "General Rules of Using Bode Plots for Impedance-Based Stability Analysis," 2018 IEEE 19th Workshop on Control and Modeling for Power Electronics (COMPEL), pp. 1–6, 2018.

Pogaku, N., Prodanovic, M., Green, T.C., 2007. Modeling, analysis and testing of autonomous operation of an inverter-based microgrid. IEEE Trans. Power Electron 22. 2, 613–625.

Ren, W., Larsen, E., 2016. A refined frequency scan approach to sub-synchronous control interaction (SSCI) study of wind farms. IEEE Trans. Power Syst. 31.5 (2016), 3904–3912.

Rygg, A., Molinas, M., Zhang, C., Cai, X., 2016. A modified sequence domain impedance definition and its equivalence to the dq-domain impedance definition for the stability analysis of ac power electronic systems. IEEE J. Emerg. Sel. Top. Power Electron. 4.4 (2016), 1382–1396.

Seyedi, Y., Karaagac, U., Mahseredjian, J., Haddadi, A., Jacobs, K., Karimi, H., 2022. Detailed modeling of inverter-based resources. In: Milano, F. (Ed.), in Advances in Power System Modelling, Control and Stability Analysis, Second ed., Ch. 5. IET Energy Engineering, pp. 175–203.

Trevisan, A.S., Mendonça, Â., Gagnon, R., Mahseredjian, J., Fecteau, M., 2021. Analytically validated SSCI assessment technique for wind parks in series compensated grids. IEEE Trans. Power Syst. 36.1 (2021), 39–48.

Watson, N., Arrillaga, J., 2003. Power Systems Electromagnetic Transients Simulation, first ed. IET, London, UK.

Webster, J.G., Amin, M., Zhang, C., Rygg, A., Molinas, M., Unamuno, E. and Belkhayat, M., "Nyquist Stability Criterion and its Application to Power Electronics Systems," Wiley Encyclopedia of Electrical and Electronics Engineering. J.G. Webster (Ed.), May 2019.

Wen, B., Boroyevich, D., Burgos, R., Mattavelli, P., Shen, Z., 2015. Small-signal stability analysis of three-phase AC systems in the presence of constant power loads based on measured d-q frame impedances. IEEE Trans. Power Electron 30.10 (2015), 5952–5963.

Xie, X., Dong, Y., Bai, K., Gao, X., Liu, P., 2012. The Improved SSR Electromagnetic Simulation Model and Its Comparison with Field Measurements. SIMULTECH 2012, Rome, Italy, pp. 419–424 (July).